The Journal of Clinical Endocrinology & Metabolism, 2026, **111**, 388–404
https://doi.org/10.1210/clinem/dgaf404
Advance access publication 14 July 2025
Clinical Research Article

Testis Molecular Pathways in CAIS Unveil Testosterone/Estradiol on Germ Cell Tumor Risk in Non-Obstructive Azoospermia

Massimo Alfano,[1] Anna Sofia Tascini,[2] Filippo Pederzoli,[1,3,†] Chiara Venegoni,[1] Irene Locatelli,[1] Arianna Lesma,[4] Giuseppe Fallara,[5,‡] Luca Boeri,[6] Edoardo Pozzi,[1,3] Fausto Negri,[1,3] Maurizio Colecchia,[7] Marina Pontillo,[8] Francesco Montorsi,[1,3] Jose Manuel Garcia-Manteiga,[2] and Andrea Salonia[1,3]

[1]Division of Experimental Oncology/Unit of Urology, URI, IRCCS Ospedale San Raffaele, Milan 20132, Italy
[2]Center for Omics Sciences, IRCCS Ospedale San Raffaele, Milan 20132, Italy
[3]Department of Urology, Università Vita-Salute San Raffaele, Milan 20132, Italy
[4]Unit of Pediatric Surgery, Department of Urology, IRCCS Ospedale San Raffaele, Milan 20132, Italy
[5]Department of Urology, IRCCS European Institute of Oncology, Milan 20141, Italy
[6]Department of Urology, Fondazione IRCCS Ca' Granda Ospedale Maggiore Policlinico, Milan 20122, Italy
[7]Department of Pathology, Università Vita-Salute San Raffaele, Milan 20132, Italy
[8]Laboratory Medicine Service, IRCCS Ospedale San Raffaele, Milan 20132, Italy

Correspondence: Massimo Alfano, PhD, Division of Experimental Oncology/Unit of Urology, URI, IRCCS Ospedale San Raffaele, Via Olgettina 60, Milan 20132, Italy. Email: alfano.massimo@hsr.it; or Anna Sofia Tascini, PhD, Center for Omics Sciences, IRCCS Ospedale San Raffaele, Via Olgettina 60, Milan 20132, Italy. Email: tascini.annasofia@unisr.it.
[†]Current address: Department of Pathology and Laboratory Medicine, Weill Cornell Medicine, New York, USA.
[‡]Current address: Division of Urology, ASST Santi Paolo e Carlo, University of Milan, Milan, Italy.

Abstract

Context: Non-obstructive azoospermia (NOA) is the most severe form of male infertility, affecting 1% of all men, with a clinical picture characterized by no sperm production, hyalinization of the basal membrane of the seminiferous tubules, primary hypogonadism, and earlier onset of age-related comorbidities compared with fertile men. NOA is also characterized by etiologic heterogeneity and the non-genetic form has higher incidence of testicular germ cell cancer (TGCC) compared to the forms with genetic abnormalities.

Objective: We aimed to establish molecular pathways in the testicular somatic cells that are either shared or specific for non-genetic and genetic forms of NOA, such as complete androgen insensitivity syndrome (CAIS) and Klinefelter syndrome (KS).

Methods: We performed single-cell RNA sequencing of the testicular somatic cells of an individual with CAIS, and data integration with published scRNA-seq datasets of testis with normal spermatogenesis, NOA, KS, and germinal testicular cancer. Detailed clinical data of the CAIS patient, testosterone and estradiol levels in age-matched men (120 fertile, 155 infertile, 116 NOA, 18 KS, and 343 with TGCC) were analyzed.

Results: In all conditions, Leydig cells are immature and senescent, but those of NOA associated with primary hypogonadism depict the highest expression of transcripts associated with the seminoma microenvironment, including estrogen-responsive genes. An oncological transcriptional signature in the Leydig cells has been confirmed at the systemic levels by showing a prognostic role of the decreasing testosterone/estradiol ratio for TGCC in men with non-genetic NOA.

Conclusion: This study offers molecular insights into the prediction of TGCC in persons with NOA and eligibility for the use of aromatase inhibitors.

Key Words: male infertility, androgen insensitivity syndrome, testis tumor, hormones, scRNA-seq

Abbreviations: AFP, alpha-fetoprotein; AMH, anti-Müllerian hormone; AUC, area under the curve; BMI, body mass index; CAIS, complete androgen insensitivity syndrome; E2, estradiol; ECLIA, electrochemiluminescence immunoassay; ECM, extracellular matrix; FSH, follicle-stimulating hormone; hCG, beta human chorionic gonadotropin; iLEY, immature Leydig cells; KS, Klinefelter syndrome; LDH, lactate dehydrogenase; LEY, Leydig; LH, luteinizing hormone; mLEY, mature Leydig cells; NOA, non-obstructive azoospermia; OR, odds ratio; ROC, receiver operating characteristic; SCOS, Sertoli cell–only syndrome; scRNA-seq, single-cell RNA sequencing; T, testosterone; TESE, testicular sperm extraction; TGCC, testicular germ cell cancer; UMI, unique molecular identifier.

Received: 28 February 2025. **Editorial Decision:** 10 July 2025. **Corrected and Typeset:** 29 July 2025

Significance Statement

This study depicts molecular pathways in the somatic testis cells of complete androgen insensitivity syndrome, and the specific and overlapping pathways with non-obstructive azoospermia and Klinefelter syndrome. The outputs from this study established a hormonal imbalance in men with non-obstructive azoospermia that is prognostic of testicular germ cell cancer.

Testicular cancer represents the most prevalent solid neoplasm in male individuals aged 15 to 39 years, with incidence rates rising 0.8% per year over the last 10 years. Overall, testicular germ cell cancers (TGCC) have an excellent curable rate, but chemotherapy or radiation treatments in young men with a long-life expectancy may negatively impact on their quality of life and fertility status (1). Impaired spermatogenesis, including non-obstructive azoospermia (NOA), with poor fertility outcomes, is one of the main features associated with testicular malignancies (2-4).

Non-obstructive azoospermia is the most severe form of male infertility affecting almost 1% of all men. Genetic defects, such as azoospermia factor c (AZFc) microdeletions in the Y chromosome and the Klinefelter syndrome (KS), only explain 15% of all male infertility cases (5). Therefore, most cases remain idiopathic in their etiology, including those with NOA. Despite the driving cause, all these forms of male infertility share some common features. Indeed, idiopathic NOA and KS share clinical characteristics, such as primary hypogonadism and earlier onset of malignant and nonmalignant noncommunicable diseases (ie, cardiovascular disease, diabetes mellitus) (2, 3, 6) compared to fertile men of the same ethnicity and comparable age (7-9). Regarding oncological disease, up to 37% of men with NOA develop TGCC (2, 3). In contrast, although men with KS have elevated risks of several cancers, a potential increased risk for TGCC has not been undoubtedly shown (10). From a pathologic standpoint, men with NOA are also characterized by immature Leydig cells and hyalinized basal membrane of the seminiferous tubules (11-13), along with imbalanced levels of sex hormones (14-16), including androgens and estrogens (17-20). An extreme phenotype of NOA is observed in the complete androgen insensitivity syndrome (CAIS), resulting in hyalinized basal membrane of the seminiferous tubule, disorder of sex development, and risk of testis malignancy (21-23).

In this study, we aimed to establish clusters of testicular somatic cell populations and molecular pathways that are shared between different forms of NOA (ie, NOA and KS) and CAIS, which could shed light on the development of prognostic markers for TGCC in azoospermic men. Hence, we carried out single-cell RNA sequencing (scRNA-seq) of the testicular somatic cells of an individual with CAIS and analyzed published scRNA-seq datasets of testis with normal spermatogenesis, NOA, KS, and TGCC.

Our findings depict molecular pathways in Leydig (LEY) cells of NOA, KS, and CAIS to be associated with immaturity, senescence, and oncological disease. The transcriptional signatures have been confirmed at both tissue and systemic levels by (i) providing evidence of indented nuclear envelope as a marker of senescence of LEY cells in NOA, KS, and CAIS; and (ii) using the analysis of peripheral level of testosterone (T) and estradiol (E2) in 627 age-matched men and 116 men with NOA, we show that 11% of men with NOA have TGCC and the T/E2 ratio is prognostic for TGCC in men with NOA.

Methods

Diagnosis of CAIS and Therapeutic Management

A 13-year old girl with 46,XY karyotype was followed for a disorder of sex development, including the occurrence of bilateral inguinal hernia at age 5, clitoral hypertrophy at age 12, and ultrasound imaging finding of a short and blind ending vaginal canal, the lack of the uterus, and fibrotic testes in place of gonads, without any anatomical alteration of the liver, gallbladder, pancreas, spleen, kidneys, bladder, and large abdominal vessels. Skeletal age was compatible with that of a female individual of the same age, as measured through x-ray bone scan and estimated by comparing with established standards of Grulich and Pyle (24). The clinical picture of CAIS was diagnosed due to HSD17B3 mutations (transversion c.277+4A>T in heterozygosis in intron 3, and intronic polymorphism c −39A>G in heterozygosis). The deficiency of HSD17B3 was confirmed by the hormonal milieu, such as high level of basal gonadotropins follicle-stimulating hormone (FSH) and luteinizing hormone (LH) associated with high level of 17-hydroxyprogesterone, and high ratio of androstenedione vs T and of T vs dihydrotestosterone. The absence of the ovaries was confirmed by undetectable levels of E2 (Table 1). Other markers indicative of the activity of the adrenal gland, as well as of the pituitary gland, the thyroid, the parathyroid, and the pancreas, were in the normal range, as well as the level of vitamins (Table 1).

Next, the patient underwent estrogen replacement therapy with LH-releasing hormone analogue (Decapeptyl) and E2 (Estraderm) since the first visit at age 13. At the age of 14, 15, 16, and 17 years, FSH and LH levels were reduced, together with drastic decrease of 17-hydroxyprogesterone, androstenedione, and T, whereas E2 and anti-Müllerian hormone (AMH) were increased. Over time, the patient was also characterized by a steady decreased level of 25-OH vitamin D (Table 1). Blood cell count, leukocyte formula, and urine analysis were always within normal ranges.

The common testicular tumoral markers levels (ie, alpha-fetoprotein [AFP], beta human chorionic gonadotropin [hCG], and lactate dehydrogenase [LDH]) remained within the reference range (Table 1). Thus, according to international guidelines, the patient underwent to bilateral orchiectomy at the age of 17. At histological analysis, the removed gonadal glands were characterized by hyalinized seminiferous tubules with hypotrophic germ cells that did not reach maturation, and the lack of LEY (Fig. 1).

Single-Cell RNA Sequencing Performance, Library Preparation, Sequencing, and Alignment

Fresh testis sample from CAIS was washed twice in phosphate-buffered saline and subjected to enzymatic digestion and assayed for scRNA-seq as reported (12). Approximately 2500 single cells were processed on the 10×

Table 1. Hormonal and metabolic profile before and after estrogen replacement therapy in CAIS

	Estrogen replacement therapy					Reference value for male ≥13 years
Age (Y)	13	14	15	16	17	
Estrogen replacement therapy	—	+	+	+	+	
FSH	45.1	2.1	1.5	<0.3	0.4	1.4-18.1 mU/mL[a]
LH	17.6	1	0.6	1.7	6.3	1.7-8.6 mU/mL[a]
17-OH-PR	2.84	0.9			0.35	0.5-2.1 ng/mL[a]
Testosterone (T)	3.79	0.23	0.24	0.31	0.33	0.28-11.1 ng/mL[a]
D4-AD	8.43	1.68	1.53	2.33	1.96	0.25-2.21 ng/mL[a]
5α-DHT	242.9	<25				250-999 pg/mL[a]
T/D4-AD	0.45					>0.8[b]
T/5α-DHT	15.6					<5[c]
INB	44.2	41.2	70.1			5-341 pg/mL[a]
Estradiol (E2)	<25	<5	9	227	240	<58 pg/mL[a]
T/E2					1.3	
AMH	1.78	9.64	22.9		7.65	0.14-12.6 ng/mL[a]
PRL	25.4				66.3	2.8-29.2 ng/mL[a]
DHEAS	2860	2280	2600		362	350-4300 ng/mL[a]
Cortisol	192	203				50-260 ng/mL[a]
p-ACTH	39	23.9				7.2-52 pg/mL[a]
FT4	1.19					0.3-1.7 ng/dL[a]
TSH	1.8			1.95	1.66	0.25-5 μU/mL[a]
p-PTH	33.9					20-90 pg/mL[a]
Insulin	10.5					2.6-25 mUI/mL[a]
Folates	6.3					>5.38 ng/mL[a]
Vit B12	607					211-911 pg/mL[a]
Vit D	39.3	39.7	23.4	25.8	17.7	20-68 ng/mL[a]
AFP		1	<0.9			<7 ng/mL[a]
hCG		<0.1	<0.2			<5 U/L[a]
LDH	203	208	200			125-220 U/L[a]

PTH and ACTH were measured in the peripheral plasma; all other analytes were measured in the peripheral serum. The estrogen replacement therapy (Decapeptyl, Estraderm) was started after the screening at age 13. The surgical removal of testis was performed at age 17.
Abbreviations: 17-OH-PR, 17-hydroxy-progesterone; 5α-DHT, dihydrotestosterone; ACTH, adrenocorticotropic hormone; AFP, alpha-fetoprotein; AMH, anti-Müllerian hormone; D4-AD, D4-androstenodione; DHEAS, dehydroepiandrosterone sulfate; FSH, follicle-stimulating hormone; FT4, free thyroxine; hCG, human chorionic gonadotropin; INB, inhibin B; LDH, lactate dehydrogenase; LH, luteinizing hormone; PRL, prolactin; PTH, parathyroid hormone; TSH, thyroid-stimulating hormone; Vit, vitamin.
[a]From the certified "Laboratory Medicine Service" of the San Raffaele Hospital.
[b]From reference (25).
[c]From reference (26).

Genomics Chromium platform, using the Single Cell 3′ Library & Gel Bead Kit v3 (10×). After quality control and quantification with the Agilent TapeStation instrument, libraries were sequenced on the Illumina NovaSeq6000 platform, generating approximately 100 000 reads per cell. Raw sequencing data were demultiplexed using Cell Ranger (v3.0.2) with the mkfastq function. Cell barcodes were identified and filtered using the whitelist and extract commands in UMI-Tools (v1.0.0), with the cell number set to 5000 using the –set-cell-number option. Reads were mapped to the GRCh38 reference genome using STAR (v2.5.3a), and gene assignment was performed with featureCounts (v1.6.4). The resulting BAM file was sorted using Samtools (v1.9). UMI-Tools count was then applied to process unique molecular identifiers (UMIs) aligned to each gene within each cell, providing distinct, error-corrected UMI counts for each gene. The UMI count table for each cellular barcode was then utilized in subsequent analyses.

Analysis of CAIS Sample

Cells type identification and clustering were conducted using Seurat (v4.4.0) in R (v4.3.3). A Seurat object was created from the UMI count table, resulting in an average of 80 000 reads per cell and a median of 1560 genes per cell. Cells that expressed fewer than 500 genes or had over 20% of reads mapping to the mitochondrial genome (percent.mt) were excluded. The remaining cells were normalized and scaled, adjusting for RNA feature counts and percent.mt effects. Principal component analysis (PCA) and unsupervised clustering were performed on the top 2000 highly variable genes using the first 20 principal components (PCs). The Seurat v4 graph-based clustering approach (using the FindNeighbours and FindClusters functions) was applied with a resolution of 0.4. Clusters were visualized through UMAP dimensional reduction using the uwot package in R. Cell identity was assigned based on cluster MGs expression reported in Fig. S1 (27).

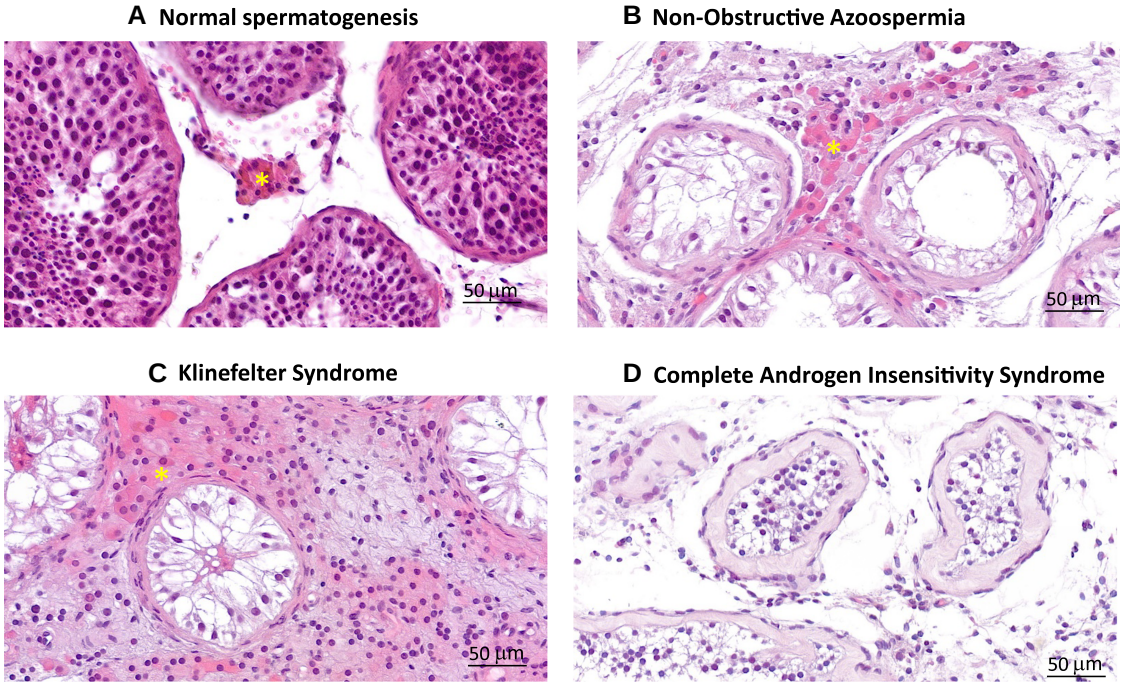

Figure 1. Testis histology. Representative morphological analysis of testicular parenchyma with normal spermatogenesis (spermatozoa at different stages of maturation in the seminiferous tubules) and clusters of LEY cells in the parenchyma obtained from a case of obstructive azoospermia due to mutation of the cystic fibrosis transmembrane conductance regulator (CFTR) gene (A), and histological analysis of testes from NOA (B), KS (C), and CAIS (D). *LEY cells. Scale bar: 50 µm.

NOA, CAIS, KS, and Control Integration, LEY-Myoid Cells Re-Clustering, and Differential Analysis on LEY Cells

We re-analyzed count matrices for 3 men with NOA (Alfano et al 2021—GSE154535), 2 men with KS (Mahyari et al 2021—GSE169062), and 9 healthy men (3 from Guo et al 2018—GSE112013, 2 from Sohni et al 2019—GSE124263, and 4 young adults from Guo et al 2022—GSE182786). Gene annotations were updated to GENCODE v31 using Ensembl IDs for consistency across versions. All these samples were integrated with our CAIS samples using the standard Seurat v4 workflow. To identify cell populations, the Seurat v4 graph-based clustering approach (using the FindNeighbours and FindClusters functions) was applied with a resolution of 0.2, and cell identities were assigned as previously described in our work (12). LEY and myoid (MYD) cells were subsetted and re-analyzed with the standard Seurat v4 workflow, using a resolution of $r = 0.3$ for cell partitioning. Differential gene expression analysis comparing all LEY cells from different pathologies (NOA, CAIS, and KS) vs healthy samples was performed using Seurat's FindMarkers function with default parameters (Wilcoxon test, logfc.threshold = 0.25, min.pct = 0.1).

Enrichment Analysis

Enrichment analysis was performed on the marker genes of each cluster in the CAIS sample (Supplementary File S1) (27) and in the LEY-MYD cells re-clustering analysis (Supplementary File S2) (27), as well as on differentially expressed genes in LEY cells across NOA, CAIS, and KS samples vs controls (Supplementary Files S3–S6) (27). Genes with a log fold change >0.25 or < −0.25 and an adjusted P value < .05 were included to identify both upregulated and downregulated pathways. Enrichment analysis used the EnrichR package (v.2.1) across databases including GO_Biological_Process_2021, GO_Cellular_Component_2021, GO_Molecular_Function_2021, Reactome_2016, KEGG_2021_Human, WikiPathways 2016, BioCarta_2016. To reduce pathway redundancy and improve interpretability, significant pathways (adj. P value < .05) were used to create Jaccard distance heatmaps for the (Figs. S1 and S2) (27). Jaccard indices, calculated with the philentropy package (v.0.5.0), provided a similarity measure between pathways, which were represented in adjacency matrices and visualized using pheatmap (v.1.0.12).

LEY Cells Development Signatures

As previously reported (12), we combined data from 3 datasets reporting scRNA-seq of neonatal, prepubertal, and adult human testes (neonatal: GSE120506; prepubertal: GSE134144; adult: GSE112013) and analyzed those according to the standard Seurat workflow. Then, we subset and re-clustered only the LEY cells, identifying 3 LEY cells at different stages of development, defined as Stage A, associated with neonatal and early prepubertal testis cells (1 and 7 years); Stage B, prepubertal testis cells (13 years); and Stage C, adult testis cells (14 and 25 years). By differential gene expression analysis, we identified the marker genes for the 3 stages and defined 3 signatures considering each cluster's top 20 most significant marker genes (Supplementary File S7) (27). Genes typically associated with spermatogenesis (ie, PRM1, PRM2, and TNP1), due to ambient RNA in adult testis, were removed from Stage C's gene signature.

Transcriptomics Signature of LEY Cell in the Context of TGCC

We re-analyzed the data from Mo et al (28), available at the GEO access number GSE197778. All 4 LEY cell sub-clusters

in the seminoma microenvironment, as identified by the authors, were combined into a single cluster (GCT-LEY). The marker genes of the GCT-LEY cluster were assessed using the Seurat function FindAllMarkers with the parameters only.pos = TRUE, min.pct = 0.25, and logfc.threshold = 0.25. The signature was defined as the top 30 expressed markers sorted by avg_log2FC.

Hematoxylin/Eosin and Immunostaining

Testis tissues with normal spermatogenesis (control [CTL]) were from men with obstructive azoospermia. Testis tissue from CTL, NOA, and KS individuals were collected from microdissection testicular sperm extraction (microTESE), as reported (12), and testis from CAIS were collected from bilateral orchiectomy. Formalin-fixed paraffin-embedded blocks were retrieved and stained using an automatic hematoxylin/eosin (HE) slide stainer (HistoCore SPECTRA ST, Leica). Immunostaining was performed on 5 µm dehydrated FFPE tissue sections after antigen retrieval, and stain as reported (12). An expert genitourinary pathologist reviewed the slides.

Nuclear Membrane Circularity

Tissues stained for CALB2 (recognition of LEY cells) and DAPI (visualization of nuclei) were assessed for the nuclear membrane circularity using a plugin in ImageJ software, whereby value 1 corresponds to a smooth nuclear surface and 0 to high levels of nuclear indentation.

Hormonal Profile

A venous blood sample was drawn from each patient between 7 AM and 11 AM, after an overnight fast, and measured as previously reported (14). The following hormones were measured by electrochemiluminescence immunoassay (ECLIA) method using the Cobas immunoanalyzer (Roche Diagnostics, Monza [MB], Italy): follicle-stimulating hormone (FSH; Roche Cat# 11775863, RRID: AB_2800499; range of linearity = 0.3-200 mUI/mL, coefficient of variability = 1.9%); luteinizing hormone (LH; Roche Cat# 11732234, RRID: AB_2800498; range of linearity = 0.3-200 mUI/mL, coefficient of variability = 2.9%); thyroid-stimulating hormone (TSH; Roche Cat# 11731459, RRID: AB_2756377; range of linearity = 0.005-100 µUI/mL, coefficient of variability = 4.7%); 17β-estradiol (E2; Roche Cat# 07027249190, RRID: AB_2920599; range of linearity = 5-3000 pg/mL, coefficient of variability = 3.9%); testosterone (T, Roche Cat# 05200067, RRID: AB_2783736; range of linearity = 0.025-15 ng/mL, coefficient of variability = 3.2%); prolactin (PRL, Roche Cat# 03203093, RRID: AB_2883976; range of linearity = 0.1-470 ng/mL, coefficient of variability = 4.3%); cortisol (Cort, Roche Cat# 06687733, RRID: AB_2802131; range of linearity = 0.054-63.4 µg/dL, coefficient of variability = 1.4%); anti-Müllerian hormone (AMH; Roche Cat# 06331076, RRID: AB_2895131; range of linearity = 0.01-23 ng/mL, coefficient of variability = 1.2%); parathyroid hormone (PTH 1-84, Roche Cat# 07027745190, RRID: AB_2895650; range of linearity = 2.4-5000 pg/mL, coefficient of variability = 1.6%); insulin (Roche Cat# 07027559, RRID: AB_2909455; range of linearity = 0.4-1000 µUI/mL, coefficient of variability = 1.4%); free beta subunit of chorionic gonadotropin (bhCG; Roche Cat# 03271749, RRID: AB_2895132; range of linearity = 0.3-190 UI/L, coefficient of variability = 1.3%); adrenocorticotropic hormone (ACTH; Roche Cat# 08946728, RRID: AB_3678556; range of linearity = 1.5-2000 pg/mL, coefficient of variability = 1.2%); dehydroepiandrosterone sulfate (DHEAS; Roche Cat# 03000087, RRID: AB_2909490; range of linearity = 0.2-1000 µg/dL, coefficient of variability = 3.2%); free thyroxine (FT4, Roche Cat#07027397190, RRID: AB_2801661; range of linearity = 0.03885-7.77 ng/dL, coefficient of variability = 1.4%); androstenedione (D4-AD; Roche Cat# 07679831190, RRID: AB_3075346; range of linearity = 0.15-10 ng/mL, coefficient of variability = 3.0%).

An enzyme-linked immunosorbent assay (ELISA) was used to measure the following hormones: inhibin B (Inhibin B Gen II Beckman Coulter Cat#A81303, RRID: AB_2827405; range of linearity = 2.6-1000 pg/mL, coefficient of variability = 4.3%); 17-OH-progesterone (17-OH-PR; DRG International Cat#EIA-1292, RRID: AB_2895664; range of linearity = 0.034-20 ng/mL, coefficient of variability = 10.0%); 5-alpha dihydrotestosterone (DHT; Tecan (IBL) Cat#DB52021, RRID: AB_2801465; range of linearity = 25-2.500 pg/ng/mL, coefficient of variability = 10.0%).

Non-Hormonal Assays

The following analytes were measured by the ECLIA method using the Cobas immunoanalyzer (Roche Diagnostics, Monza (MB), Italy): vitamin B12 (Vit B12; Roche Cat# 07028121190, range of linearity = 100-2000pg/mL, coefficient of variability = 2.3%); folate (Folate; Roche Cat# 07027290190, range of linearity = 0.6-20 pg/mL, coefficient of variability = 2.2%); Vitamin D (Vit D; Roche Cat# 09038078, range of linearity = 6-120 ng/mL, coefficient of variability = 3.0%); alpha-fetoprotein (AFP; Roche Cat# 07026706190, range of linearity = 0.908-1210 ng/mL ng/mL, coefficient of variability = 1.0%); lactate dehydrogenase (LDH; Roche Cat# 05169330, range of linearity = 10-1000 U/L, coefficient of variability = 1.1%).

Statistical Methods

We applied receiver operating characteristic (ROC) curve analysis to evaluate the predictive accuracy of the T/E2 ratio. The area under the curve (AUC) was calculated with 95% CI to quantify discriminative ability. The optimal cutoff value was determined using the Youden index (maximum sensitivity + specificity − 1). To assess the clinical utility of this marker at the identified threshold, we performed decision-curve analysis to quantify the net benefit across a range of clinically relevant threshold probabilities.

Ethics

Data collection followed the principles outlined in the Declaration of Helsinki; all patients signed an informed consent agreeing to provide their own anonymous information and tissue specimens. The informed consent for the person with CAIS was signed by the parents. The study was approved by the Institutional Review Board (Ethics Committee IRCCS Ospedale San Raffaele, Milan, Italy), and was composed of 2 protocols for collecting data and using bio-specimens from infertile (Authorization Protocol Infertilità-2015, amended on March 2016) and fertile men

(Authorization Protocol URIMALES-2016, further amended on March 2018), and 1 protocol for biobanking (Authorization Protocol URI001-2010, further amended on December 2015 and April 2019). All methods were carried out in accordance with the approved guidelines.

Results

Histology of Testes With Normal Spermatogenesis, NOA, and KS

Specimens of testis parenchyma of men with normal spermatogenesis, NOA, and KS were obtained by microTESE. The testis with normal spermatogenesis of a case with obstructive azoospermia was used as a reference, showing sperm cells at different stages of maturation in the seminiferous tubules and cluster of LEY cells in the parenchyma (Fig. 1A). Conversely, testes from NOA and KS were characterized by sclerosis of the basement membrane of the seminiferous tubules, absence of germ cells compatible with Sertoli cell–only syndrome (SCOS) and the presence of hyperplastic LEY cells (Fig. 1B and 1C).

Histology of Testis With CAIS

The diagnosis of CAIS (21) was based on the clinical picture of androgen insensitivity syndrome due to HSD17B3 mutations (transversion c.277+4A>T in heterozygosis in intron 3, and intronic polymorphism c−39A>G in heterozygosis). The deficiency of HSD17B3 was confirmed by the hormonal milieu, that is, high basal FSH and LH levels associated with high level of 17-hydroxyprogesterone, along with high ratio of androstenedione/T and of T vs dihydrotestosterone. Likewise, the diagnosis was confirmed because of a phenotype characterized by the disorder of sex development at puberty (Table 1). To prevent testicular malignancy (22), and to promote the development of the female phenotype and female gender identity, this individual underwent 4-year estrogen replacement therapy (29) before testis removal at age of 17 years and continued the same therapy (Decapeptyl FL 3.75 mg every 84 days, Estraderm—Estreva gel 3 puffs/day) after orchiectomy. Four years after estrogen replacement therapy, T/E2 ratio was 1.3 (Table 1), similar to what reported in women (about 5) (30) during the reproductive age. The morphological analysis of the testicular parenchyma depicted the presence of sclerosis of the basement membrane of the seminiferous tubules, and the absence of germ cells, thus being compatible with SCOS, as previously reported for men with androgen insensitivity syndrome due to androgen receptor mutations (22), as well as for NOA and KS. Furthermore, CAIS was characterized by the absence of recognizable LEY cells in testicular parenchyma (Fig. 1D).

ScRNA-seq of CAIS Testis

We performed single-cell RNA sequencing on a freshly isolated specimen of CAIS testis. After filtering out poor-quality cells, a total of 2558 somatic cells were analyzed. The Seurat standard graph-based clustering approach was used for cell partitioning and cluster identification, and the 7 identified cell clusters shown in the UMAP (31) plot (Fig. 2A). The main somatic cell populations were identified using previously determined cell type marker genes (32, 33) (Fig. 2B). More than 50% of somatic cells expressed markers of LEY cells, and 3 subpopulations were identified as mature LEY (mLEY that included INSL3 among the top 10 marker genes), immature LEY (iLEY that included DLK1 among the top 10 marker genes) and cells with a mix phenotype of peritubular myoid (LEY/MYD) cells. Moreover, the other populations were macrophages (MCR), pericytes (PER), Sertoli (SRT) and endothelial cells. Of note was the lack of a clear population of MYD cells (Fig. 2C).

To deepen the characterization of the LEY/MYD population and of each somatic cell population in the CAIS case (Fig. 2D), we applied functional enrichment analysis to the specific marker genes of each cluster (Fig. 2E, Supplementary File S1 (27)). Of the pathways specific for LEY/MYD cells, the "smooth muscle cell contraction" allowed us to define this cell cluster as classical peritubular cells, although with a mixed phenotype with that of LEY. This cell cluster with mixed characteristics may be explained by the common origin of LEY and MYD cells from the embryonal mesonephron (34), and the incomplete differentiation of MYD that normally mature at puberty in response to increased androgen production (35). The phenotype of LEY/MYD has been shown to persist in human testis until puberty, then segregating into LEY and MYD (36, 37) cells. Other pathways that were specific for the LEY/MYD cells included response to and the metabolism of metal ions, which could represent a consequence of an incomplete maturation of the LEY cells and the stage-specific expression of metal ion binding protein (38).

Likewise, iLEY cells showed characteristics of fetal LEY cells in the undifferentiated state producing androstenedione—present at a very high level in this 17-year-old patient (Table 1)—which is converted to T by HSD17B3 (39), indeed mutated in this individual. Furthermore, iLEY cells were enriched also for the pathways of regulation of the "complement activation," "immune response," and "cellular senescence."

Pathways specific to mLEY were all related to the synthesis of steroid and cholesterol. The mLEY cells, compared to the iLEY and LEY/MYD populations, were enriched for pathways upstream T synthesis, as steroids and cholesterol biosynthesis, which can be explained by increased feedback due to the lack of T synthesis in this individual, because of the presence of HSD17B3 mutations.

As expected, macrophages were enriched for specific pathways related to the immune system and endothelial cells were enriched for specific pathways related to vasculogenesis, respectively. Sertoli cells were enriched for pathways associated to male gonad development and apoptosis, and pericytes were enriched for pathways associated to smooth muscle contraction and cellular adhesion, respectively.

Integration of CAIS Sample With NOA, KS, and Normal Spermatogenesis

To investigate the molecular pathways associated with the impaired T/E2 ratio, we also analyzed published data (Table 2 and Table S1 (27)) from 9 control (CTL) adult testicular tissues reported in a study that analyzed 10 327 testis somatic cells (32, 40, 41), 3 testis samples from men with NOA for a total of 3860 somatic cells (12), and testis tissue from 2 men with KS for a total of 4227 somatic cells (42), by applying the same cell partitioning protocol used for the CAIS sample. After data integration, 7 cell clusters were identified and represented for all conditions (Fig. 3A). Concerning the resident immune cells, the presence of the cell cluster identified as

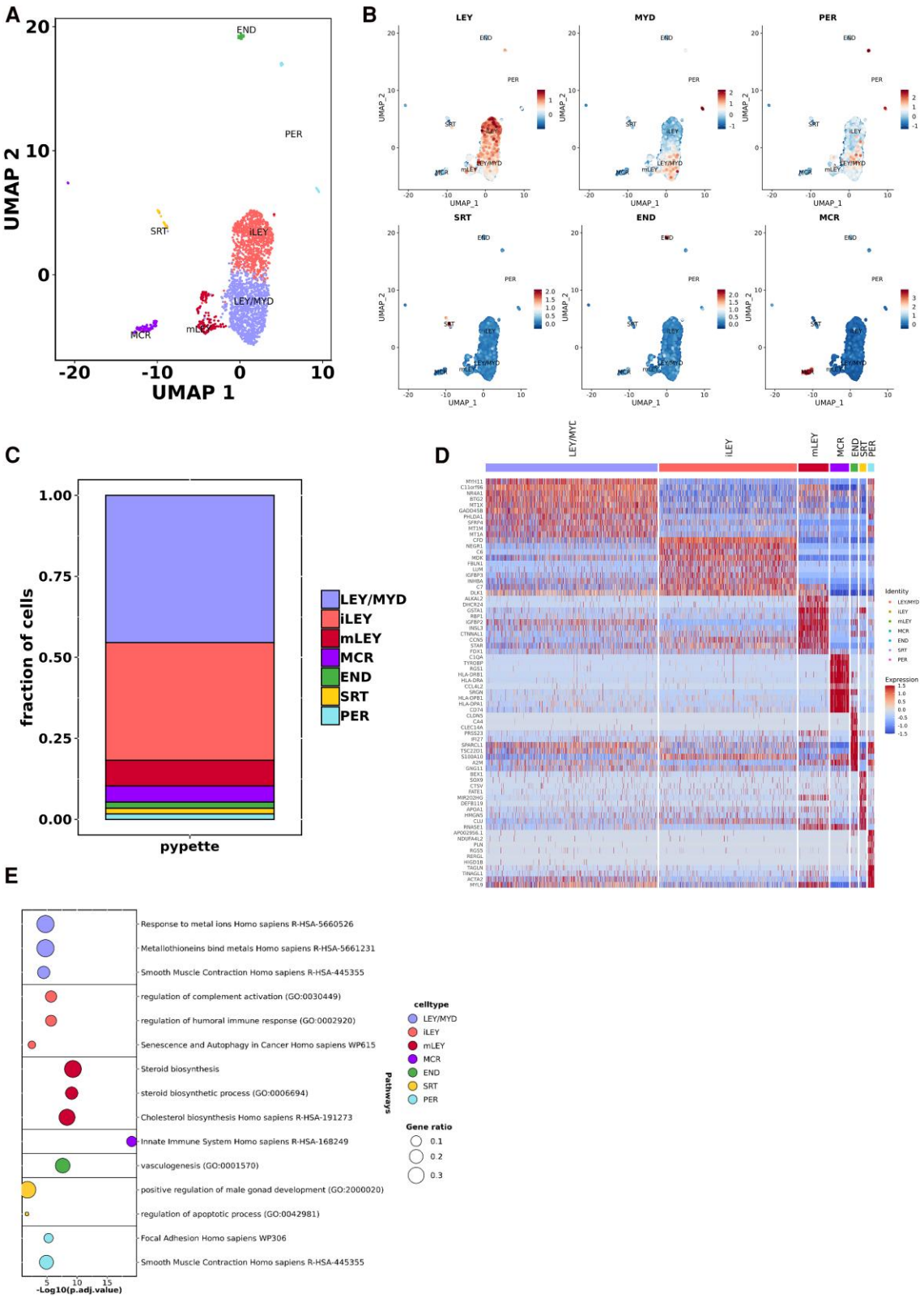

Figure 2. ScRNA-seq of the testis from an individual with Morris syndrome. A) UMAP plot at resolution of 0.4 representing testis cells from a tissue sample of CAIS patient. B) UMAP plots showing the expression patterns of selected marker genes used to identify testis cell types. C) Relative abundance of cell populations in CAIS sample. D) Heatmap showing the expression signature of the top 10 expressed genes in each cluster. E) Selection of significant pathways from Supplementary File S1 for each cluster (27).

T lymphocytes (TCL), that was absent in the CTL and CAIS, was particular to the azoospermic groups with NOA and KS, while macrophages were present in all conditions (Fig. 3B). Likewise, endothelial cells were present in all conditions, with a proportional representation of pericytes in all conditions (Fig. 3B). Similarly, MYD and SER cells were also

Table 2. Sample sizes and sources employed in each type of analysis carried out in this study

ScRNA-seq	n	References
Complete androgen insensitivity syndrome (CAIS)	1	GSE298368
Re-analysis of scRNA-seq published datasets		
Normal spermatogenesis	9	(32, 40, 41)
LEY immature	7	(32, 36, 40)
LEY in seminoma environment	1	(28)
KS	2	(42)
NOA	3	(12)
Peripheral level of testosterone and estradiol in men		
Fertile	120	This study
Idiopathic infertile	155	This study
KS	18	This study
NOA	103	This study
NOA with TGCC	13	This study
TGCC	50	This study
	293	(43)

Details about ScRNA-seq datasets are reported in Table S1. (27)
Abbreviations: KS, Klinefelter syndrome; LEY, Leydig cells; NOA, NON-OBSTRUCTIVE azoospermia; TGCC, testicular germ cell cancer.

present in all conditions, although less represented in KS (Fig. 3B). A striking difference was in the relative abundance of LEY cells in disease tissue vs CTL condition (Fig. 3B).

Since we have noted a pathway toward impaired differentiation of LEY cells associated with an abnormal T/E2 ratio in CAIS, we hypothesized that this hormonal ratio could be representative of the degree of mature/immature stage of the testis somatic cells. We assayed the stage of differentiation of LEY cells in the entire cohort of men; thus, the transcriptional signatures of the early, intermediate, and late stages of LEY cell differentiation (A, B, and C, respectively) were extracted from available datasets (32, 36) (Supplementary File S7 (27)) and tested within the transcriptional profiles of LEY cells of our cohorts. Of all, controls have a greater expression of the Stage C signature, which is typical of the postpubertal maturation stage (Fig. 3C). Non-obstructive azoospermia cells were stuck at stage B (pubertal) and characterized by the overexpression of several genes involved in the extracellular matrix (ECM) organization; this process is particularly relevant since hyalinization of the seminiferous tubules is present in the testis of adult men with NOA, and these findings allow us to hypothesize that this process already begins at the pubertal stage. LEY cells of the infertile groups characterized by a genetic condition, namely, KS and CAIS, were stuck at stage A (neonatal) and characterized by cellular response to cytokines; furthermore, the transcriptional profile of LEY cells of KS was also enriched in terms of negative regulation of transcription from RNA polymerase II promoter in response to stress (Fig. 3D).

Re-Clustering of LEY and MYD Cells

Having shown that CAIS was characterized by the presence of mixed LEY/MYD subpopulation, we re-clustered LEY and MYD cells from all cohorts of testis to explore cell subpopulations in the other cohorts. We identified 8 cell subpopulations (Fig. 4A) that were differently distributed among the 4 cohorts (Fig. 4B). Cluster 5 was present only in CAIS, and cluster 7 only in KS (Fig. 4B). Cluster 6 was enriched in azoospermic men (ie, NOA and KS) vs CTL (Fig. 4B).

Functional enrichment analysis showed that cluster 5 was enriched for the Oncostatin M Signaling Pathway, cell response to cytokines and negative regulation of the cell cycle. Cluster 7 was enriched for several pathways associated with the formation and transport of membrane vesicles from the ER to the Golgi apparatus and MHC protein complex. Cluster 6 was enriched for pathways related to the intracellular storage of iron ions and protein synthesis (Fig. 4C, Supplementary File S2 (27)).

The 8 cell subpopulations in the CAIS revealed that the cluster 5 was composed of LEY/MYD (Fig. 4D), in agreement with previous reports showing that LEY/MYD mature to LEY and MYD after male puberty (36, 37), a condition that was not reached in the individual with CAIS and was even inhibited by the 4 years of estrogen replacement therapy. In conclusion, the re-clustering of LEY and MYD cells allowed us to appreciate the existence of a peculiar subpopulation of LEY cells only in the CAIS, which has a phenotype of LEY/MYD and characterized by the Oncostatin M Signaling Pathway.

Shared Upregulated and Downregulated Pathways in the LEY Cells of Infertile Men

Functional enrichment analysis was used to identify those gene ontologies and pathways in LEY cells shared among CAIS, KS, and NOA individuals vs those with normal spermatogenesis (Supplementary Files S3 and S4 (27) for upregulated pathways, Supplementary Files S5 and S6 (27) for downregulated pathways). Jaccard distance heatmaps were used to group and select the pathways (Fig. S2 (27) for upregulated pathways, Fig. S3 (27) for downregulated pathways), and the most representative gene ontologies were reported in the heatmaps.

Men with KS represented the cohort with the highest number of upregulated pathways, followed by NOA and CAIS. The upregulated pathways shared among the 3 cohorts of infertile individuals constituted 7.8% (Fig. 5A). Among the 3 conditions, the shared upregulated pathways in LEY cells were related to Oncostatin M, Senescence and autophagy in cancer and TGFb signaling (Fig. 5B), all of them associated with cellular senescence and aging-related pathology (44, 45).

Men with KS also represented the cohort with the highest number of downregulated pathways, followed by NOA and CAIS. The number of downregulated pathways shared among the 3 cohorts of infertile individuals represented 8.9% (Fig. 5C). Among the 3 conditions, the shared downregulated pathways in LEY cells were related to (i) focal adhesion, which includes cell-substrate junction associated to down-modulation of surface protein such as integrin β1 and CD151, and homotypic cell-cell adhesion that are indicative of poorly differentiated cell phenotype; and (ii) elastic fiber formation as downregulated expression of ECM proteins elastin, Microfibril Associated Protein 2, Latent Transforming Growth Factor Beta Binding Proteins and TGFB1 (Fig. 5D).

Therefore, despite different maturation stages and differences among different populations, LEY cells from these men are shared (Supplementary results) (27).

Senescence of LEY Cells in NOA, KS, and CAIS

The transcriptional profile of LEY cells in all analyzed conditions (ie, NOA, KS, and CAIS) revealed a phenotype associated with cellular senescence. We found that the nuclear envelope of

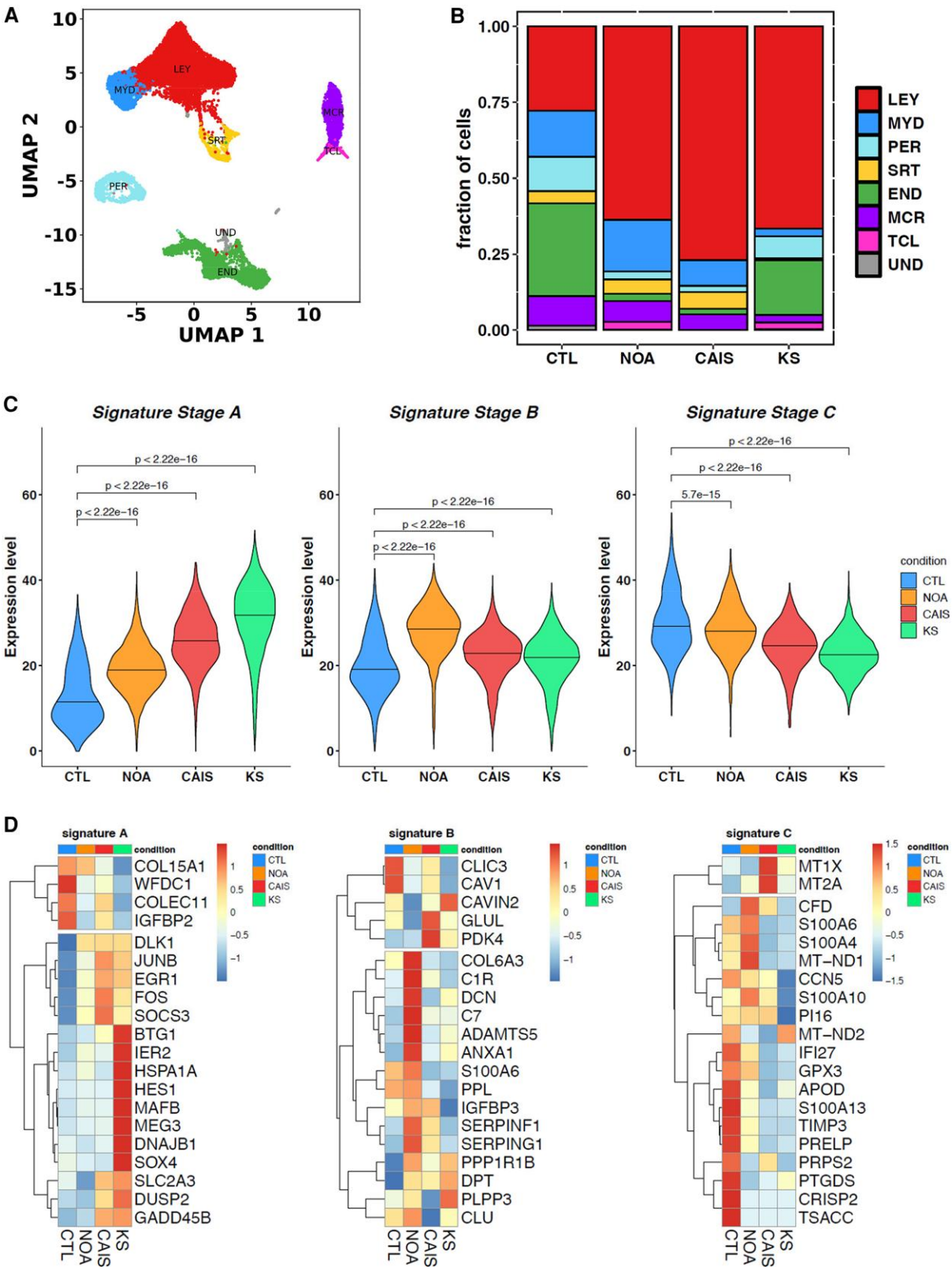

Figure 3. Integration of CAIS sample with NOA, KS, and CTL from the literature. A) UMAP plot resulting from the integration of somatic testis cells of CAIS with 3 samples of NOA, 2 samples of KS, and 9 samples of normal CTL reported in Table S2 (27). B) Relative abundance of cell populations in CTL, NOA, CAIS, and KS samples. C) Violin plots compare expression levels of Stage A–C signatures of LEY cell maturation in CAIS, NOA, and KS vs healthy donor (2-sided Mann Whitney test). Signatures were established by combining 3 datasets reporting single-cell RNA seq of neonatal, prepubertal, and adult human testis analysis recently detailed (12); for the CAIS sample all LEY phenotypes (mLEY, iLEY, and LEY/MYD) were pulled together. D) Heatmaps showing the average expression of the genes in the 3 stages signatures of LEY with hierarchical clustering of genes. Heatmaps were produced with the R library *pheatmap v1.0*.

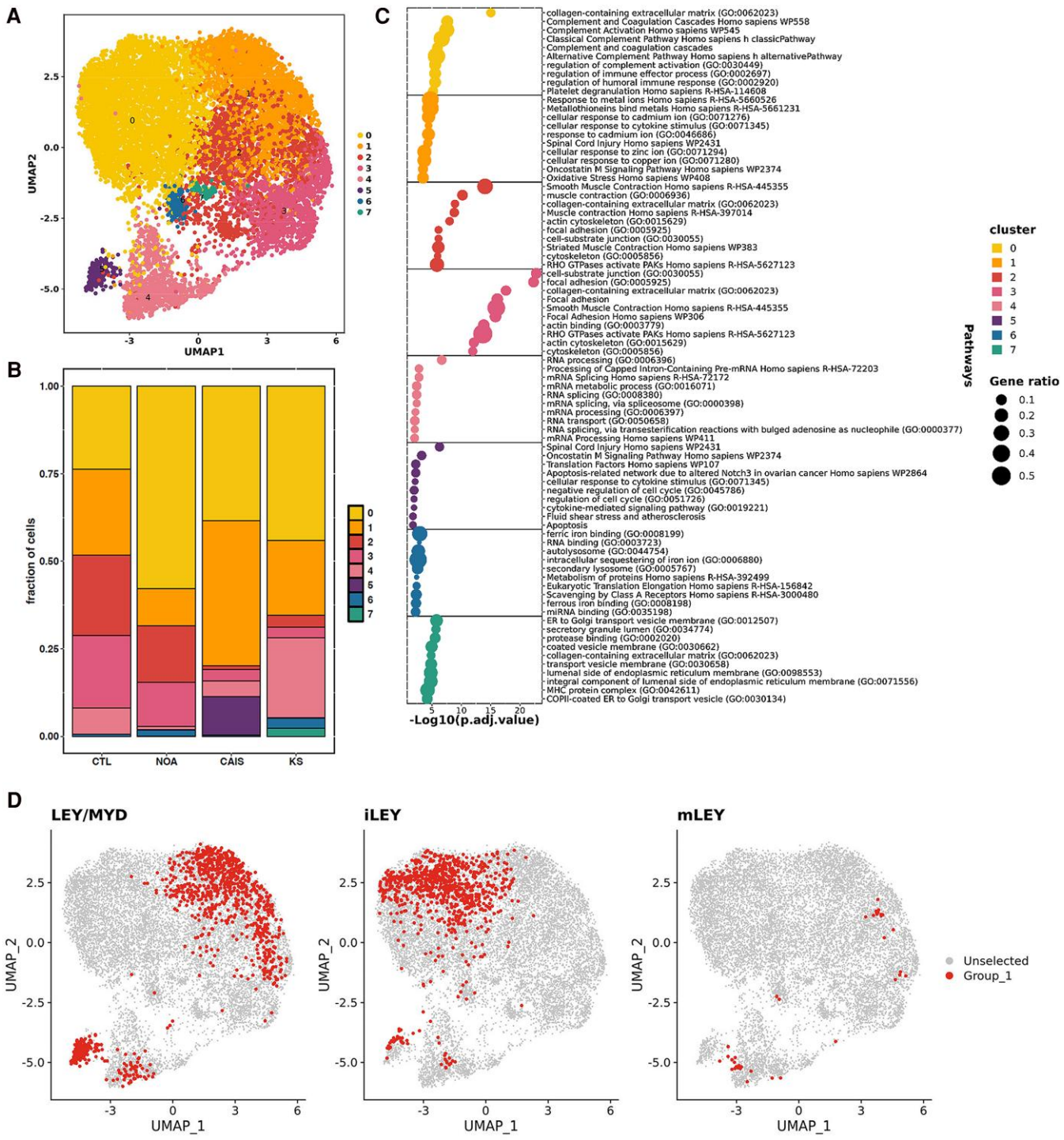

Figure 4. Re-clustering of LEY and MYD cells. A) UMAP plot showing the re-clustering of integrated LEY and MYD cells from CAIS, NOA, KS, and CTL samples. B) Relative abundance of cell subpopulations in LEY-MYD re-clustering. C) Top 10 most significant pathways enriched from the marker genes of the 8 clusters derived from LEY-MYD re-clustering (Supplementary File S3) (27). D) UMAP plots highlighting the 3 clusters of LEY cells in CAIS samples (LEY/MYD, iLEY, and mLEY) across LEY-MYD sub-clusters of cells.

LEY cells in all diseased conditions was distorted compared to control LEY cells in the testis with normal spermatogenesis, with nuclear envelopes significantly more indented than LEY cells CTL, as assessed by the nuclear circularity parameter (Fig. 5E). Likewise, the shape and invagination of nuclear envelope reported here for LEY cells of NOA, KS, and CAIS are reminiscent of nuclei structure observed in aging and senescence, as well as in patients with nuclear envelopathies (46).

LEY Cells From Men With NOA Express Gene Signature Associated With Seminoma Microenvironment

From the analysis of the shared pathways, for all pathological conditions (ie, NOA, KS, and CAIS), the LEY cells showed a phenotype associated to cancer (ie, Oncostatin M, TGF-B signaling and decreased cell-cell and cell-matrix adhesion). To deepen the characterization of LEY cells in the disease

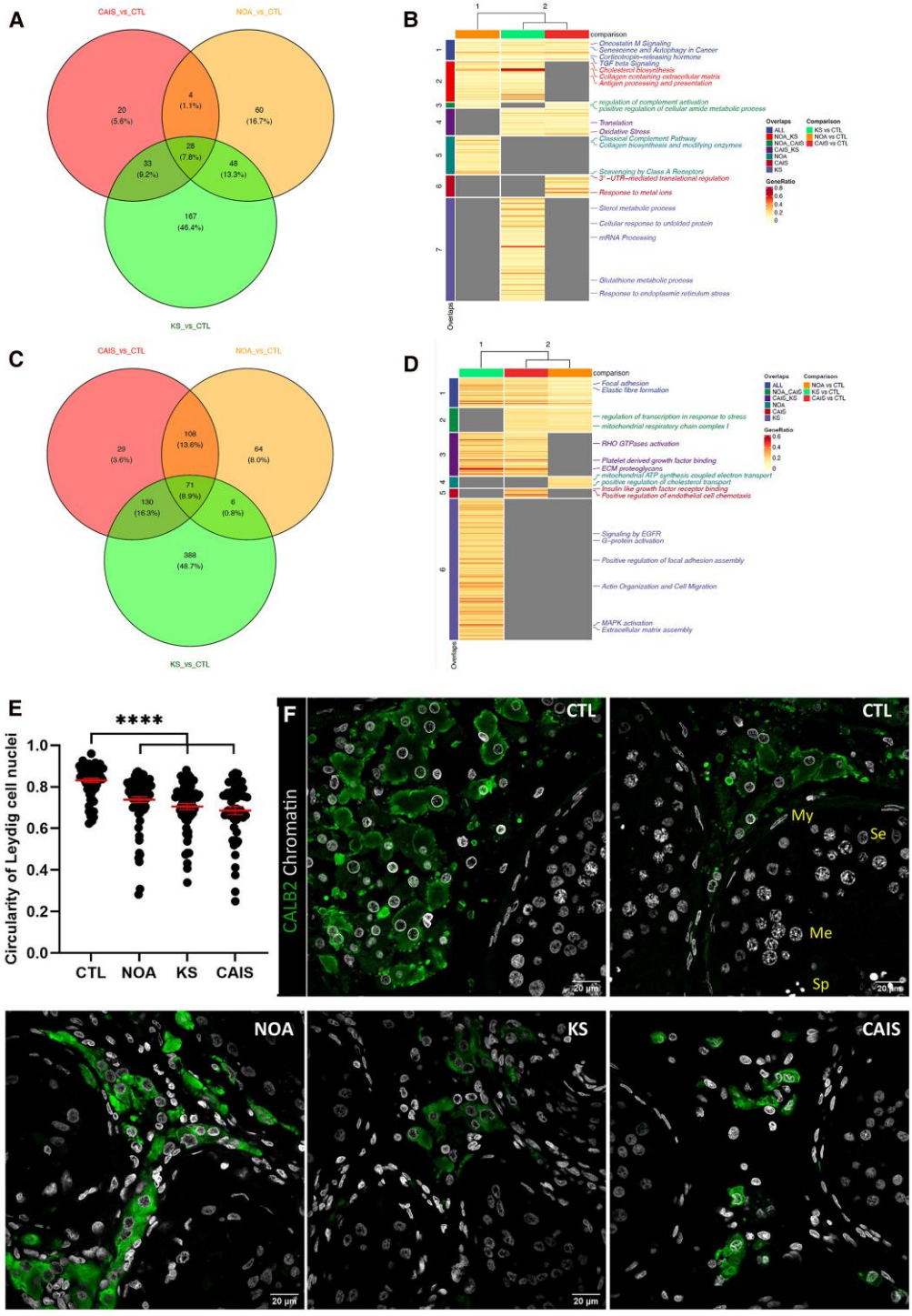

Figure 5. Senescence phenotype of LEY cells in NOA, KS, and CAIS. A) Venn diagram of the intersection of up-modulated pathways enriched in LEY cells for the comparisons CAIS vs CTL, NOA vs CTL, and KS vs CTL. The pathways were filtered out for p.adj value higher than 0.05, and at least 5 modulated genes (Supplementary Files S3 and S4) (27). B) The pathways passing the gene ratio filter >10% were used to plot the heatmap. Pathways were placed in a custom order to highlight pathways shared among conditions or specific to one condition. C) Venn diagram of the intersection of downmodulated pathways enriched in LEY cells for the comparisons CAIS vs CTL, NOA vs CTL, and KS vs CTL. The pathways were filtered out for p.adj value higher than 0.05, and at least 5 modulated genes (Supplementary Files S5 and S6) (27). D) The pathways passing the gene ratio filter >20% were used to plot the heatmap. Pathways were placed in a custom order to highlight pathways shared among conditions or specific to one condition; pathways shared between NOA and KS are not reported because they did not pass the gene ratio filter. E) Quantification of the circularity of the nuclear envelope of LEY cells, as proxy for nuclear envelope deformation in NOA, KS, and CAIS. CTL, n = 4 independent donors both for a total of 97 LEY cells; NOA, n = 4 independent donor for a total of 86 LEY cells; KS, n = 3 independent donors both for a total of 62 LEY cells; CAIS, n = 1 independent donor for a total of 54 LEY cells. Red bars represent mean ± SEM; ANOVA test. F) Representative images used for the quantification of the circularity of the nuclear envelope of LEY cells. LEY cells were identified by immunofluorescence staining of lineage-specific marker CALB2, and chromatin by DAPI. Two representative images of the testis parenchyma with normal spermatogenesis from 2 independent donors showing the regular shape of the nuclear envelope of LEY cells, and one image representative of the testis parenchyma of NOA, KS, and CAIS showing the presence of several nuclei of LEY cells with indented nuclear envelope. Sperm cells (Sp), meiotic cells (Me), peritubular myoid cells (My), and Sertoli cells (Se) that are recognized for the presence of a characteristic DAPI-negative condensed nucleolus.

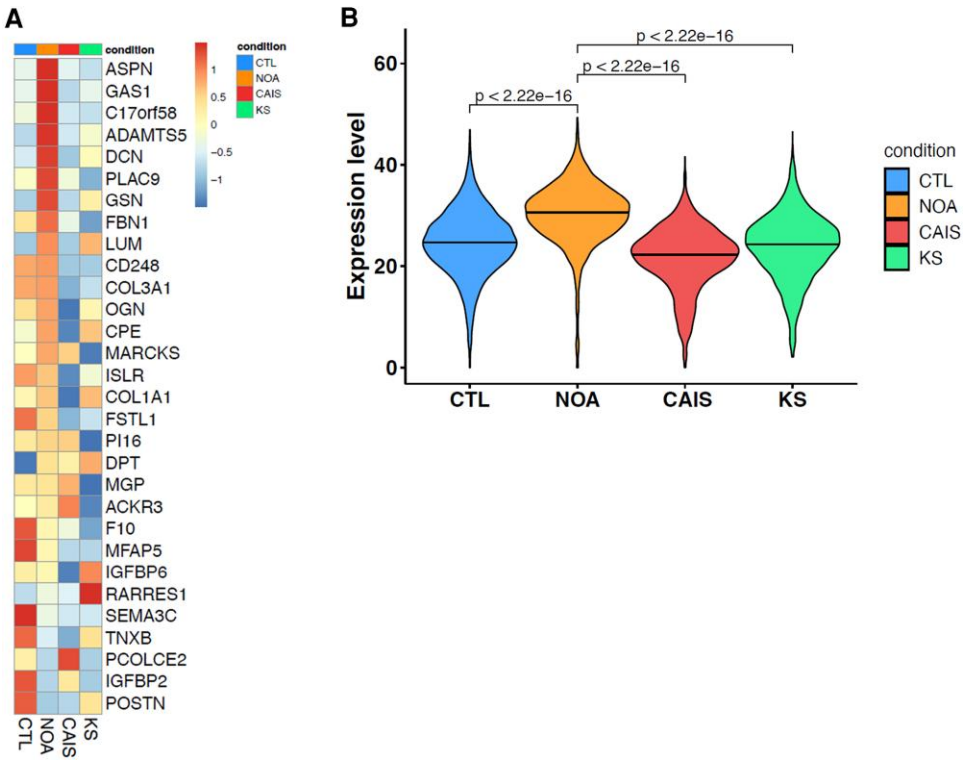

Figure 6. LEY cells from men with NOA express gene signature associated with seminoma microenvironment. Heatmap showing the expression level of the most differentially expressed genes by LEY cells in the context of seminoma, among LEY cells in our cohorts (A). Violin plot showing the average expression level of the GCT signature of LEY cells for condition, with statistical analysis for each group vs NOA condition (B).

conditions, we extracted the transcriptional signatures from scRNA-seq of LEY cells isolated from a testis with metastatic seminoma (28) and compared it to the transcriptional profiles of LEY cells in our cohorts (Fig. 6A).

The LEY cells of NOA have the greatest rate of overexpression of germ cell tumor-associated transcriptomic signature compared to the other cohorts (Fig. 6B). This information is in agreement with clinical reports; indeed, in CAIS individual, the testes are usually removed to prevent the occurrence of testicular malignancies; KS individuals have elevated risks of several cancers, but not testis (10); moreover, among all infertile categories, men with NOA are those with the highest risk of developing TGCC (2, 3). Of the deregulated transcriptional signature in NOA LEY cells, several gene products are engaged in the extracellular matrix assembly (Col 1A1, LUM, CD248, COL 3A1, OGN, ADAMTS5, Decorin, Asporin, Fibrilln 1, C17orf58), and cell adhesion to ECM (POSTN, TNXB, SEMA3C). Furthermore, men with NOA, of the modulated genes in the LEY cells of the CPE, COL1A1, and GAS1 have been reported to be modulated by estrogens (47-49).

Testosterone/Estradiol Ratio Is Decreased Both in Men With NOA and Men With TGCC

LEY cells are the primary site of T production and conversion to E2 by the Aromatase P450 (CYP19A1). The impact of altered balance between sexual hormones has been reported and represents the basis of sexual dimorphism and infertility (50). Thereof, we speculated that T/E2 ratio could be used as a marker of LEY function in men with idiopathic infertility, thus including NOA.

Several reports showed the levels of sex hormones in infertile men compared to age-matched individuals, but without reporting the fertility status of the control group. Here, we measured the levels of sex hormones in age-matched men with proven fertility and infertility status (Table 2). Testosterone and E2 levels were measured from blood samples collected between 7 and 10 AM in a fasting state from a total of 374 men aged 18 to 42 years, as follows: 120 fertile men (median [IQR] age 35 years [32-38]); 155 men with idiopathic male factor infertility (37 years [34-40]); 103 men with NOA (36 years [33-40]); and 18 men with KS (37 years [32-39]), respectively.

A significant and gradual decrease in T levels was demonstrated in non-NOA infertile men, men with NOA, and men with KS, as compared with fertile men. In contrast, a gradual increase was observed for the E2 levels (Fig. 7A and 7B). The ratio between T and E2 was then established, after normalizing the unit of measurement using the formula (T*1000)/E2). The T/E2 ratio was found to be reduced in idiopathic infertile vs fertile men and further reduced in men with NOA (Fig. 7C), thus indicating that men with NOA expressed the greatest hormonal imbalance among idiopathic infertile men. The T/E2 ratio was further reduced in NOA due to a genetic background, as in the men with KS (Fig. 7C).

In addition to the 103 men with NOA reported above, 9 NOA men (35 years [32-41]), who had been referred for couple infertility and underwent microTESE, were diagnosed with TGCC at the time of surgery. The whole cohort did have conventional tumoral markers (ie, LDH, AFP, and hCG) within the normal range. Moreover, suspected testicular masses were found in 4 patients with NOA at ultrasound investigation throughout the diagnostic workup and the testes were removed during onco-microTESE due to seminomas at

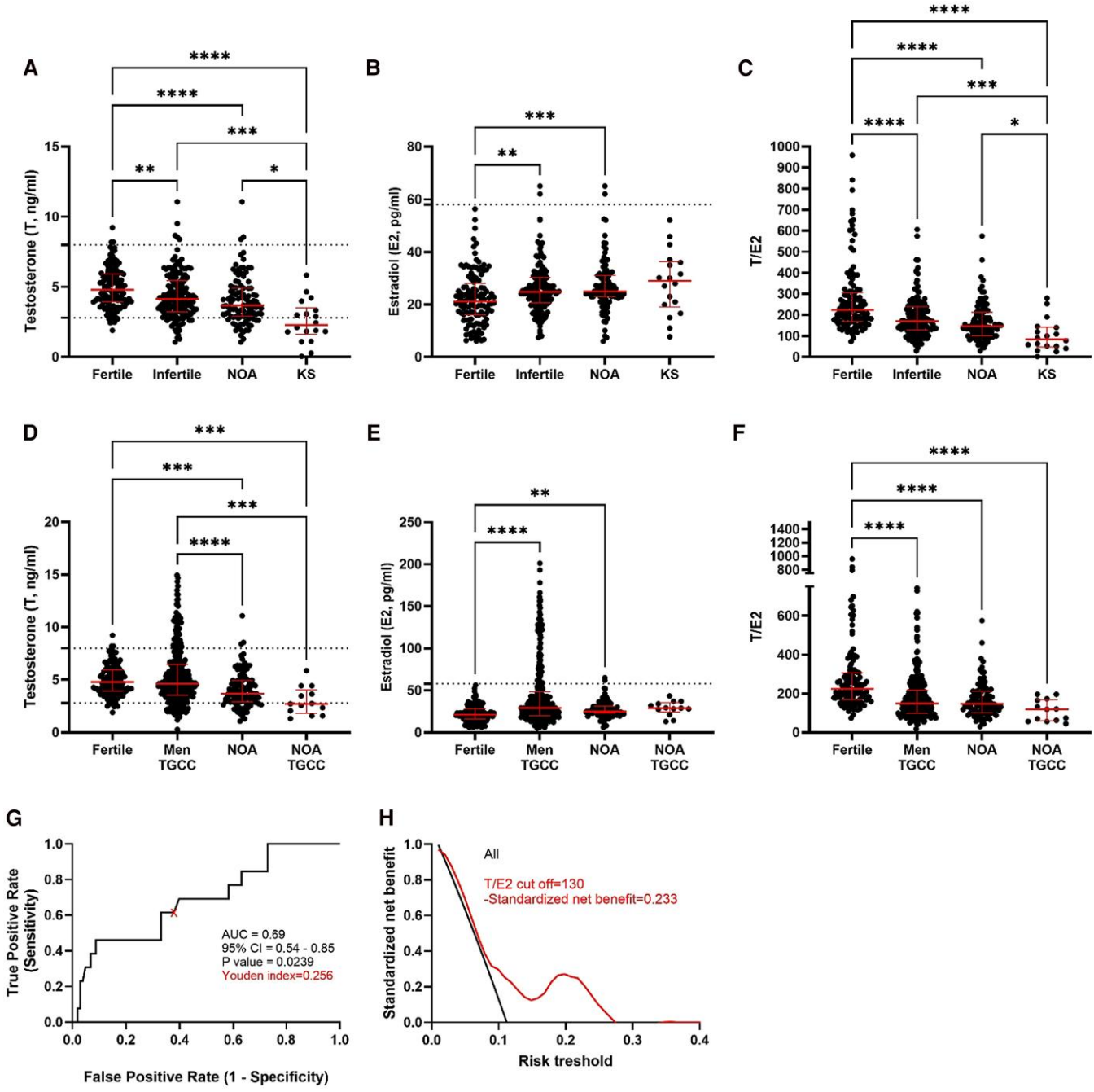

Figure 7. Sex hormones. Peripheral level of T, E2, and T/E2 ratio were established in the blood sample of fertile and infertile men in the absence of any neoplastic disease (A-C), and in the NOA with TGCC and TGCC alone (D-F); the data for the cohort "Men TGCC" are from the pool of data from OSR dataset and publicly available dataset (43). Red lines show median and interquartile range. Dotted lines show reference value. ROC-derived curve, showing the AUC, 95% CI, statistical significance, and the optimal Youden index (G). Decision curve analysis showing the standardized net benefit of T/E2 ratio value of 130 on the prediction of TGCC in NOA men (H).

frozen sections. Overall, our cohort consisted of 13 men with concomitant NOA and TGCC.

To establish the clinical relevance of T/E2 ratio in the context of TGCC, we compared the T/E2 ratio measured in fertile men vs a cohort of age-matched men with a confirmed TGCC. The TGCC cohort comprised 50 men enrolled at the same Institute and by the re-analysis of a cohort from a public dataset consisting of 293 men with a pathologically confirmed TGCC (43). The 2 cohorts were comparable in terms of age, T and E2 levels, and T/E2 ratio (Fig. S4) (27). Thereof, data were pulled together for a total of 343 men with TGCC. The T/E2 ratio in fertile non-neoplastic men was the highest compared to all other tested conditions (223 [169-306]) and constantly decreased in men with TGCC (148 [98-216]), with NOA (147 [101-212]) and with both NOA and TGCC (119 [59-168]) (Fig. 7D-7F). No significant difference was identified among the cohorts of men with disease (Fig. 7D-7F).

Predictive Role of T/E2 for TGCC in NOA

Univariable and multivariable logistic regression models were used to assess the potential role of T/E2 ratio to predict the

risk of men with NOA to develop TGCC. Both NOA men with and without malignancies were used (Table S2) (27). At univariable analysis, lower levels of T (odds ratio [OR] = 0.571; 95% CI = 0.326-0.9; $P = 0.03$) and of T/E2 ratio (OR = 0.987; 95% CI = 0.976-0.998; $P = .0289$) were associated with the presence of TGCC (Table S3) (27). The analysis was then implemented for possible confounders such as age and body mass index (BMI), as both parameters can have an impact on the extra-gonadal conversion of T to E2 due to the expression of the aromatase P450 in extra-gonadal organs, including fat tissue (51). After adjusting for those variables, the T/E2 ratio was still independently associated with TGCC in men with NOA, regardless of BMI (OR = 0.987; 95% CI = 0.974-0.997; $P = .028$) or age (OR = 0.987; 95% CI = 0.974-0.997; $P = .028$) (Table S4) (27).

To quantify discrimination of TGCC in men with NOA based on T/E2 ratio, the AUC of the ROC-curve was estimated (Fig. 7G), with AUC of 0.69 (95% CI: 0.54-0.85, $P = .0239$). Using the Youden index (J = 0.256), we identified an optimal cutoff value of 130 for the T/E2 ratio, corresponding to a sensitivity of approximately 0.62 and specificity of 0.64. The decision-curve analysis revealed that using the T/E2 ratio with the established cutoff of 130 provided a standardized net benefit of 0.233 across clinically relevant risk thresholds (Fig. 7H).

Using the T/E2 ratio at the cutoff value of 130, this model would result in a net gain of 23 true positives for every 100 patients, after accounting for the harm of false positives. The T/E2 ratio at the cutoff value of 130 helps identify meaningful cases of TGCC in patients with NOA while avoiding unnecessary interventions in most non-cases. The T/E2 model offered superior net benefit compared to the "treat all" approach for risk thresholds between approximately 0.05 and 0.3, with the greatest relative advantage observed in the threshold range of 0.15 to 0.25.

Discussion

This study reports the first scRNA-seq analysis of the testis in an individual with CAIS phenotype, associated with a X-linked recessive condition due to natural mutations of the enzyme HSD17B3 responsible for T production. The relevance of such a dataset resides in the fact that it derives from a natural mutation that impairs T production, and the clinical management of this individual with estrogen therapy recapitulates a few of the conditions observed in men with NOA, such as the unbalanced T/E2 ratio in both men with NOA and KS. Comparison among scRNA-seq datasets unveils pathways that allow a better understanding of NOA, and particularly those forms not associated with genetic abnormalities.

The analysis of upregulated/downregulated pathways revealed that LEY cells senescence occurs among NOA (12), KS, and CAIS individuals. The relationship between cellular senescence and interaction with ECM has only recently been unveiled, but further reports show that decreased focal adhesion signaling induces cellular senescence (52) and fibrosis in the experimental autoimmune orchitis-induced senescence of LEY cells (53).

Unbalanced composition of the ECM of the basal membrane of the seminiferous tubules has been reported for NOA (13). In agreement, our data showed that testicular parenchyma of men with NOA, KS, and CAIS is characterized by fibrosis (ie, hyalinization of the basal membrane of the seminiferous tubules and increased TGFB signaling by LEY cells) and an unbalanced composition of the ECM. Moreover, LEY cells are senescent and undifferentiated, although the stage of maturation is different between NOA (stage B, prepubertal) and KS and CAIS (stage A, neonatal).

In addition to the pathways shared with NOA and KS, indicating an unbalanced ECM composition, the increased response to metal ions is peculiar for the LEY cells from CAIS. This pathway is indicative of a cellular response to the accumulation of metal ions in the extracellular space, to maintain metal homeostasis and to avoid cytotoxicity (54). Accumulation of divalent metal ions has been reported in association with ECM remodeling and tumor invasion (55); these sets of pathways in the CAIS testis could also be representative of a neoplastic-like environment, as potentially suggested by the high frequency of testicular malignancy in prepubertal and pubertal patients with AIS (56).

The strength of this study was the analysis of a substantial cohort of infertile and age- and ethnicity-matched fertile individuals to establish the actual role of T/E2 ratio. Of infertile categories, the azoospermic men are those with the highest risk of developing testis cancer, ranging between 10% and 37% for those with SCOS (2, 3). Moreover, LEY cells hyperplasia and dysfunction have been associated with TGCC (57, 58). The histological analysis and the relative abundance of LEY cells by scRNA-seq showed LEY cells hyperplasia in KS and NOA, which is related to their degree of differentiation at the prepubertal stage. Our findings agree with the above studies, supporting the association between LEY cells hyperplasia and the presence of a testicular neoplastic microenvironment in azoospermic men.

Other than producing T, LEY cells are the primary site where T is converted to E2 by the action of aromatase P450 (*CYP19A1*), although other extra-gonadal organs expressing the aromatase P450 could contribute to the conversion of T to E2 in men (51). In men with NOA, LEY cells are characterized by very high levels of CYP19A1 (59) and their impaired steroidogenesis is associated with hyperplasia (60). Likewise, in the preclinical model the expression of human aromatase was shown to be responsible for low T levels and high E2 levels; the increased E2 level has an autocrine/paracrine effect and is responsible for LEY cell immaturity, LEY hyperplasia, cryptorchidism, and infertility (61-63), and an increased incidence of TGCC (64). Of note, TGCC cells express several estrogen receptors, making this neoplasia estrogen-dependent for tumor development and growth (65). Since T/E2 ratio is independent from age and BMI, the interpretation of our findings is that T/E2 ratio is a marker of testis dysfunction in men with NOA, with a potential role of LEY cells with a transcriptomic profile associated to the presence of TGCC as marker, which is not diagnosed by the conventional tumor markers. The potential role of the neoplastic phenotype of LEY cells in NOA, represented by the overexpression of several genes responsible for ECM assembly, seems similar to what occurs for the modulation of fibroblasts into cancer-associated fibroblasts in a neoplastic microenvironment.

The cellular pathways expressed by LEY cells indicate that they are stuck at an immature stage, which, at the same time, is senescent in NOA, CAIS, and KS. For CAIS and KS, these phenotypes are associated with gene mutations and are unrelated to the neoplastic microenvironment. In the case of NOA, LEY cells phenotype could be a representation of pro-neoplastic

microenvironment, which is reflected by a decreased T/E2 ratio. Sex hormones also regulate the differentiation and activity of the immune system, with estrogens associated with clinical manifestations of autoimmune diseases while androgens having a protective effect (66, 67). Further studies would investigate the potential association between the T/E2 ratio and the incidence of immune-related disease in infertile men (68). Likewise, the T/E2 ratio can also help to identify those patients who could benefit the most from the use of aromatase inhibitors, thus aiming to increase T levels and potentially improve the fertility status (69). In men with NOA this strategy could be applied as a neoadjuvant treatment before TESE to increase the chance of sperm retrieval. Likewise, aromatase inhibitors could be potentially used to reduce the incidence of TGCC in men with NOA and low T/E2 ratio. A potential clinical implication of this information is that T/E2 ratio could be easily used in men to design a counseling path to monitor the status of the testis parenchyma, and in azoospermic men as a predictor of TGCC development (68, 70).

The incorporation of external datasets enhances the robustness of the study, but it also can introduce variability due to discrepancies in sample processing, sequencing platforms, and analytical methodologies. To overcome the bias of using different scRNA-seq datasets, we applied the same criteria for the selection of raw data, such as the use of the same platform and good quality of sequencing (ie, cell count and percentage of mitochondrial genes) and applied the same strategy for the analysis.

Although having homogeneous cohorts of White-European men, a major limitation of this study is that different geographic areas and ethnicity groups might increase variance in terms of T/E2 ratio. To improve the relevance of T/E2 ratio, hormone dosage can be improved by standardizing the blood collection. When evaluating the clinical use of sex hormones, their circadian variation must be considered, particularly for T (71). Thus, it is relevant that both sex hormones can be measured in the same blood sample collected in a fasting state between 7 AM and 10 AM, when T and E2 have their peak of production (71).

Another potential limitation is the limited number of TGCC events in the NOA cohort, which warrants future validation in external cohorts across different clinical centers and ethnic populations.

Acknowledgments

We thank Dr. Cesare Covino (ALEMBIC, IRCCS Ospedale San Raffaele) for technical support.

Funding

This work was supported by URI-Urological Research Institute free funds; the funding source did not have any role in the present study.

Disclosures

All authors declare no competing interests.

Data Availability

The authors confirm that the data supporting the findings of this study are available within the article and its supplementary material (27). The single-cell RNA sequencing data generated in this study (one testis from an individual with complete androgen insensitivity syndrome, CAIS) have been deposited in the GEO database under accession code "GSE298368." The testicular cells scRNA-seq data from published datasets are reported in Table 2, and the re-analysis of those datasets deposited in the GEO database under accession code "GSE298368."

References

1. Lobo J, Gillis AJM, Jeronimo C, Henrique R, Looijenga LHJ. Human germ cell tumors are developmental cancers: impact of epigenetics on pathobiology and clinic. *Int J Mol Sci*. 2019;20(2):258.
2. Mancini M, Carmignani L, Gazzano G, *et al*. High prevalence of testicular cancer in azoospermic men without spermatogenesis. *Hum Reprod. Apr*. 2007;22(4):1042-1046.
3. Maiolino G, Fernandez-Pascual E, Ochoa Arvizo MA, Vishwakarma R, Martinez-Salamanca JI. Male infertility and the risk of developing testicular cancer: a critical contemporary literature review. *Medicina (Kaunas)*. 2023;59(7):1305.
4. Del Giudice F, Kasman AM, Berardinis D, *et al*. Association between male infertility and male-specific malignancies: systematic review and meta-analysis of population-based retrospective cohort studies. *Fertil Steril*. 2020;114(5):984-996.
5. Krausz C, Escamilla AR, Chianese C. Genetics of male infertility: from research to clinic. *Reproduction*. 2015;150(5):R159-R174.
6. Glazer CH, Bonde JP, Eisenberg ML, *et al*. Male infertility and risk of nonmalignant chronic diseases: a systematic review of the epidemiological evidence. *Semin Reprod Med*. 2017;35(3):282-290.
7. Kanakis GA, Nieschlag E. Klinefelter syndrome: more than hypogonadism. *Metabolism*. 2018;86:135-144.
8. Bojesen A, Juul S, Birkebaek NH, Gravholt CH. Morbidity in Klinefelter syndrome: a Danish register study based on hospital discharge diagnoses. *J Clin Endocrinol Metab*. 2006;91(4):1254-1260.
9. Price WH, Clayton JF, Wilson J, Collyer S, De Mey R. Causes of death in X chromatin positive males (Klinefelter's syndrome). *J Epidemiol Community Health*. 1985;39(4):330-336.
10. Swerdlow AJ, Schoemaker MJ, Higgins CD, Wright AF, Jacobs PA, Group UKCC. Cancer incidence and mortality in men with Klinefelter syndrome: a cohort study. *J Natl Cancer Inst*. 2005;97(16):1204-1210.
11. Di Persio S, Neuhaus N. Human spermatogonial stem cells and their niche in male (in)fertility: novel concepts from single-cell RNA-sequencing. *Hum Reprod*. 2023;38(1):1-13.
12. Alfano M, Tascini AS, Pederzoli F, *et al*. Aging, inflammation and DNA damage in the somatic testicular niche with idiopathic germ cell aplasia. *Nat Commun*. 2021;12(1):5205.
13. Alfano M, Pederzoli F, Locatelli I, *et al*. Impaired testicular signaling of vitamin A and vitamin K contributes to the aberrant composition of the extracellular matrix in idiopathic germ cell aplasia. *Fertil Steril*. 2019;111(4):687-698.
14. Alfano M, Ventimiglia E, Locatelli I, *et al*. Anti-mullerian hormone-to-testosterone ratio is predictive of positive sperm retrieval in men with idiopathic non-obstructive azoospermia. *Sci Rep*. 2017;7(1):17638.
15. Pozzi E, Corsini C, Belladelli F, *et al*. Role of follicle-stimulating hormone, inhibin B, and anti-mullerian hormone in predicting sperm retrieval from men with nonobstructive azoospermia undergoing microdissection testicular sperm extraction: a systematic review and meta-analysis. *Eur Urol Open Sci*. 2024;65:3-12.
16. Pozzi E, Raffo M, Negri F, *et al*. Anti-mullerian hormone predicts positive sperm retrieval in men with idiopathic non-obstructive azoospermia-findings from a multi-centric cross-sectional study. *Hum Reprod*. 2023;38(8):1464-1472.
17. Tao Y. Endocrine aberrations of human nonobstructive azoospermia. *Asian J Androl*. 2022;24(3):274-286.
18. Salama N, Blgozah S. Serum estradiol levels in infertile men with non-obstructive azoospermia. *Ther Adv Reprod Health* 2020;14:2633494120928342.

19. De Rocco Ponce M, Selice R, Di Mambro A, De Toni L, Foresta C, Garolla A. Estradiol-testosterone imbalance is associated with erectile dysfunction in patients with Klinefelter syndrome. *J Clin Med*. 2021;10(11):2319.
20. Pacenza N, Pasqualini T, Gottlieb S, *et al.* Clinical presentation of Klinefelter's syndrome: differences according to age. *Int J Endocrinol*. 2012;2012:324835.
21. Mains LM, Vakili B, Lacassie Y, Andersson S, Lindqvist A, Rock JA. 17beta-hydroxysteroid dehydrogenase 3 deficiency in a male pseudohermaphrodite. *Fertil Steril*. 2008;89(1):228.e13-2228.e7.
22. Kaprova-Pleskacova J, Stoop H, Bruggenwirth H, *et al.* Complete androgen insensitivity syndrome: factors influencing gonadal histology including germ cell pathology. *Mod Pathol*. 2014;27(5):721-730.
23. Cools M, Looijenga L. Update on the pathophysiology and risk factors for the development of malignant testicular germ cell tumors in complete androgen insensitivity syndrome. *Sex Dev*. 2017;11(4):175-181.
24. Alshamrani K, Offiah AC. Applicability of two commonly used bone age assessment methods to twenty-first century UK children. *Eur Radiol*. 2020;30(1):504-513.
25. Phelan N, Williams EL, Cardamone S, *et al.* Screening for mutations in 17beta-hydroxysteroid dehydrogenase and androgen receptor in women presenting with partially virilised 46,XY disorders of sex development. *Eur J Endocrinol*. 2015;172(6):745-751.
26. Starka L, Pospisilova H, Hill M. Free testosterone and free dihydrotestosterone throughout the life span of men. *J Steroid Biochem Mol Biol*. 2009;116(1-2):118-120.
27. Alfano M, Tascini AS, Pederzoli F, *et al.* Supplementary information for "Testis Molecular Pathways in CAIS Unveil Testosterone/Estradiol on Germ Cell Tumor Risk in Non-Obstructive Azoospermia". *San Raffaele Open Research Data Repository, V1*. 2025. https://doi.org/10.17632/gh6mhbzjj5.1
28. Mo L, Yu Z, Lv Y, *et al.* Single-cell RNA sequencing of metastatic testicular seminoma reveals the cellular and molecular characteristics of metastatic cell lineage. *Front Oncol*. 2022;12:871489.
29. Gottlieb B, Trifiro MA. Androgen insensitivity syndrome. In: Adam MP, Mirzaa GM, Pagon RA, *et al.* eds. *GeneReviews®* [Internet]. University of Washington, Seattle; 1993. Updated May 11, 2017. https://www.ncbi.nlm.nih.gov/books/NBK1429/
30. Dimitrakakis C, Zhou J, Bondy CA. Androgens and mammary growth and neoplasia. *Fertil Steril*. 2002;77(Suppl 4):S26-S33.
31. Becht E, McInnes L, Healy J, *et al.* Dimensionality reduction for visualizing single-cell data using UMAP. *Nat Biotechnol*. 2018;37:38-44.
32. Guo J, Grow EJ, Mlcochova H, *et al.* The adult human testis transcriptional cell atlas. *Cell Res*. 2018;28(12):1141-1157.
33. Xia B, Yan Y, Baron M, *et al.* Widespread transcriptional scanning in the testis modulates gene evolution rates. *Cell*. 2020;180(2):248-262.e21.
34. Wen Q, Cheng CY, Liu YX. Development, function and fate of fetal Leydig cells. *Semin Cell Dev Biol*. 2016;59:89-98.
35. Palombi F, Farini D, Salanova M, de Grossi S, Stefanini M. Development and cytodifferentiation of peritubular myoid cells in the rat testis. *Anat Rec*. 1992;233(1):32-40.
36. Guo J, Nie X, Giebler M, *et al.* The dynamic transcriptional cell atlas of testis development during human puberty. *Cell Stem Cell*. 2020;26(2):262-276.e4.
37. Guo J, Sosa E, Chitiashvili T, *et al.* Single-cell analysis of the developing human testis reveals somatic niche cell specification and fetal germline stem cell establishment. *Cell Stem Cell*. 2021;28(4):764-778.e4.
38. Jauregui EJ, Mitchell D, Garza SM, Topping T, Hogarth CA, Griswold MD. Leydig cell genes change their expression and association with polysomes in a stage-specific manner in the adult mouse testis. *Biol Reprod*. 2018;98(5):722-738.
39. O'Shaughnessy PJ, Baker PJ, Heikkila M, Vainio S, McMahon AP. Localization of 17beta-hydroxysteroid dehydrogenase/17-ketosteroid reductase isoform expression in the developing mouse testis–androstenedione is the major androgen secreted by fetal/neonatal leydig cells. *Endocrinology*. 2000;141(7):2631-2637.
40. Sohni A, Tan K, Song HW, *et al.* The neonatal and adult human testis defined at the single-cell level. *Cell Rep*. 2019;26(6):1501-1517.e4.
41. Nie X, Munyoki SK, Sukhwani M, *et al.* Single-cell analysis of human testis aging and correlation with elevated body mass index. *Dev Cell*. 2022;57(9):1160-1176.e5.
42. Mahyari E, Guo J, Lima AC, *et al.* Comparative single-cell analysis of biopsies clarifies pathogenic mechanisms in Klinefelter syndrome. *Am J Hum Genet*. 2021;108(10):1924-1945.
43. Torzsok P, Oswald D, Dieckmann KP, *et al.* Subsets of preoperative sex hormones in testicular germ cell cancer: a retrospective multicenter study. *Sci Rep*. 2023;13(1):14604.
44. Tominaga K, Suzuki HI. TGF-beta signaling in cellular senescence and aging-related pathology. *Int J Mol Sci*. 2019;20(20):5002.
45. La Belle AA, Schiemann WP. Oncostatin M activation of Stat3:Smad3 complexes drives senescence. *Cell Cycle*. 2017;16(6):497-498.
46. Gauthier BR, Comaills V. Nuclear envelope integrity in health and disease: consequences on genome instability and inflammation. *Int J Mol Sci*. 2021;22(14):7281.
47. Zeng Y, Ma WK, Li LJ, *et al.* Identification and validation of eight estrogen-related genes for predicting prognosis of papillary thyroid cancer. *Aging (Albany NY)*. 2023;15(5):1668-1684.
48. Leavy M, Trottmann M, Liedl B, *et al.* Effects of elevated beta-estradiol levels on the functional morphology of the testis—new insights. *Sci Rep*. 2017;7(1):39931.
49. Nishi K, Fu W, Kiyama R. Novel estrogen-responsive genes (ERGs) for the evaluation of estrogenic activity. *PLoS One*. 2022;17(8):e0273164.
50. Lahimer M, Abou Diwan M, Montjean D, *et al.* Endocrine disrupting chemicals and male fertility: from physiological to molecular effects. *Front Public Health*. 2023;11:1232646.
51. Barakat R, Oakley O, Kim H, Jin J, Ko CJ. Extra-gonadal sites of estrogen biosynthesis and function. *BMB Rep*. 2016;49(9):488-496.
52. Shin EY, Park JH, You ST, *et al.* Integrin-mediated adhesions in regulation of cellular senescence. *Sci Adv*. 2020;6(19):eaay3909.
53. Li Y, Mi P, Wu J, *et al.* High throughput scRNA-Seq provides insights into Leydig cell senescence induced by experimental autoimmune orchitis: a prominent role of interstitial fibrosis and complement activation. *Front Immunol*. 2021;12:771373.
54. Cherian MG, Jayasurya A, Bay BH. Metallothioneins in human tumors and potential roles in carcinogenesis. *Mutat Res*. 2003;533(1-2):201-209.
55. Stelling MP, Motta JM, Mashid M, Johnson WE, Pavao MS, Farrell NP. Metal ions and the extracellular matrix in tumor migration. *FEBS J*. 2019;286(15):2950-2964.
56. Barros BA, Oliveira LR, Surur CRC, Barros-Filho AA, Maciel-Guerra AT, Guerra-Junior G. Complete androgen insensitivity syndrome and risk of gonadal malignancy: systematic review. *Ann Pediatr Endocrinol Metab*. 2021;26(1):19-23.
57. Tarsitano MG, Bandak M, Jorgensen N, *et al.* Quantification of the Leydig cell compartment in testicular biopsies and association with biochemical Leydig cell dysfunction in testicular cancer survivors. *Andrology*. 2018;6(5):748-755.
58. Colecchia M, Nistal M, Gonzalez-Peramato P, *et al.* Leydig cell tumor and hyperplasia: a review. *Anal Quant Cytol Histol*. 2007;29(3):139-147.
59. Adamczewska D, Slowikowska-Hilczer J, Walczak-Jedrzejowska R. The fate of Leydig cells in men with spermatogenic failure. *Life (Basel)*. 2022;12(4):570.
60. Lardone MC, Argandona F, Florez M, *et al.* Overexpression of CYP19A1 aromatase in Leydig cells is associated with steroidogenic dysfunction in subjects with Sertoli cell-only syndrome. *Andrology*. 2017;5(1):41-48.

61. Li X, Nokkala E, Yan W, *et al*. Altered structure and function of reproductive organs in transgenic male mice overexpressing human aromatase. *Endocrinology*. 2001;142(6):2435-2442.
62. Abney TO. The potential roles of estrogens in regulating Leydig cell development and function: a review. *Steroids*. 1999;64(9):610-617.
63. Strauss L, Kallio J, Desai N, *et al*. Increased exposure to estrogens disturbs maturation, steroidogenesis, and cholesterol homeostasis via estrogen receptor alpha in adult mouse Leydig cells. *Endocrinology*. 2009;150(6):2865-2872.
64. O'Donnell L, Robertson KM, Jones ME, Simpson ER. Estrogen and spermatogenesis. *Endocr Rev*. 2001;22(3):289-318.
65. Fenichel P, Chevalier N. Is testicular germ cell cancer estrogen dependent? The role of endocrine disrupting chemicals. *Endocrinology*. 2019;160(12):2981-2989.
66. Santana-Sanchez P, Vaquero-Garcia R, Legorreta-Haquet MV, Chavez-Sanchez L, Chavez-Rueda AK. Hormones and B-cell development in health and autoimmunity. *Front Immunol*. 2024;15:1385501.
67. Aguilar-Pimentel JA, Cho YL, Gerlini R, *et al*. Increased estrogen to androgen ratio enhances immunoglobulin levels and impairs B cell function in male mice. *Sci Rep*. 2020;10(1):18334.
68. Fallara G, Pozzi E, Belladelli F, *et al*. A systematic review and meta-analysis on the impact of infertility on men's general health. *Eur Urol Focus*. 2024;10(1):98-106.
69. Pozzi E, Venigalla G, Raymo A, *et al*. Eligibility for the medical therapy among men with non-obstructive azoospermia-findings from a multi-centric cross-sectional study. *Andrology*. 2024;13:234-242.
70. Boeri L, Ventimiglia E, Cazzaniga W, *et al*. Risk of health status worsening in primary infertile men: a prospective 10-year follow-up study. *Andrology*. 2022;10(1):128-136.
71. Brambilla DJ, Matsumoto AM, Araujo AB, McKinlay JB. The effect of diurnal variation on clinical measurement of serum testosterone and other sex hormone levels in men. *J Clin Endocrinol Metab*. 2009;94(3):907-913.